



Article

Magnetoelectric Transducer Designs for Use as Wireless Power Receivers in Wearable and Implantable Applications

Tyrel Rupp ¹, Binh Duc Truong ², Shane Williams ² and Shad Roundy ²,*

- ¹ Space Dynamics Laboratory, Utah State University, Logan, UT 84322, USA; tyrel.rupp@gmail.com
- Department of Mechanical Engineering, University of Utah, Salt Lake City, UT 84112, USA; Binh.D.Truong@utah.edu (B.D.T.); shanewill1234@gmail.com (S.W.)
- * Correspondence: shad.roundy@utah.edu; Tel.: +1-801-581-4304

Received: 14 January 2019; Accepted: 1 February 2019; Published: 8 February 2019



Abstract: As the size of biomedical implants and wearable devices becomes smaller, the need for methods to deliver power at higher power densities is growing. The most common method to wirelessly deliver power, inductively coupled coils, suffers from poor power density for very small-sized receiving coils. An alternative strategy is to transmit power wirelessly to magnetoelectric (ME) or mechano-magnetoelectric (MME) receivers, which can operate efficiently at much smaller sizes for a given frequency. This work studies the effectiveness of ME and MME transducers as wireless power receivers for biomedical implants of very small ($<2~\text{mm}^3$) size. The comparative study clearly demonstrates that under existing safety standards, the ME architecture is able to generate a significantly higher power density than the MME architecture. Analytical models for both types of transducers are developed and validated using centimeter scale devices. The Institute of Electrical and Electronics Engineers (IEEE) and the International Commission on Non-Ionizing Radiation Protection (ICNIRP) standards were applied to the lumped elements models which were then used to optimize device dimensions within a 2 mm³ volume. An optimized ME device can produce $21.3~\text{mW/mm}^3$ and $31.3~\text{\muW/mm}^3$ under the IEEE and ICNIRP standards, respectively, which are extremely attractive for a wide range of biomedical implants and wearable devices.

Keywords: wireless power transfer; magnetoelectric transducers; piezoelectric transducers; biomedical implants

1. Introduction

The current explosion of wearable devices has led to increased attention on methods to power them from harvested energy. Implantable Medical Devices (IMDs) might be considered a natural extension of wearable devices especially in the context health related applications. This paper will discuss methods to wirelessly transmit power to IMDs. However, the same methods and devices could easily be applied to wearable devices in order to enhance their usability.

Currently, the most common way to power IMDs is via a direct (wired) external source or a battery implanted along with the IMD. Direct power delivery may cause limitations to patient mobility and creates medical risks associated with passing wires transcutaneously. Batteries help mitigate the problems presented by the direct powering method, however they have finite lifetimes and require periodic replacement. This concern is particularly relevant as the sensing and computation components of IMDs become very small (i.e., 1 mm³ or smaller). In light of these concerns, a Wireless Power Transfer (WPT) system would appear to be a promising solution.

Acoustic WPT systems have recently been investigated largely due to the fact that acoustic power has low attenuation in soft tissue and short wavelengths (compared to electromagnetic wavelengths)

Materials **2019**, 12, 512 2 of 18

which increases the efficiency of very small receivers. However, acoustic power transfer systems are complicated by poor transmission through bone and the need for the transmitter to be in direct contact with the skin [1]. For a detailed review of acoustic WPT systems applied to IMDs the reader is referred to [2].

Electromagnetic WPT systems have been widely investigated for use by IMDs. For the purposes of this paper, we classify electromagnetic WPT as either Inductive Power Transfer (IPT) if the coupling is in the near field, or Radio Frequency (RF) if the coupling is in the mid field (i.e., transition region) or far field. Inductive coupling techniques appear to be the most advanced for powering implants. Inductive coupling utilizes a pair of coils that must be physically close and well aligned to allow for the transfer of power. Subsequently, the power transfer is highly dependent on the size, orientation, and distance between the coils [3]. Ultimately, these dependencies make this form of WPT most viable for IMDs (such as pacemakers [4]) where the depth of the implant is relatively shallow and the alignment of the coils can be well controlled.

Unlike acoustic and inductively coupled systems, alignment is not as critical for RF WPT systems because receivers do not need to be tightly coupled to the transmitter. However, as the size of receivers decrease, the operating frequency must increase to a level where tissue tends to absorb and attenuate the transmitted signal [5]. This attenuation is not only inefficient, but it is potentially hazardous because of associated tissue heating. A technology that could make efficient use of low frequency electromagnetic power transfer at a distance could be a significant enabler for very small implantable systems. Magnetoelectric (ME) transducers could be such a technology.

The magnetoelectric effect refers to any type of coupling between electric and magnetic fields found in matter [6]. The ME effect was first demonstrated experimentally in 1960 when Dzyaloshinskii witnessed it in Cr_2O_3 [7]. Despite this breakthrough, subsequent research showed that at best the magnetoelectric coefficient for bulk materials such as Cr_2O_3 was very low, on the order of $100 \text{ mV/(cm} \cdot Oe)$ [7]. This, along with other various complications, kept the materials from being used much in practical applications [6]. Before the ME effect was even observed in bulk materials, Tellegen suggested developing composites that demonstrated a cumulative ME effect [8]. The implication here is that by coupling two separate physical effects (piezoelectric (PE) and magnetostrictive (MS)) in two separate materials an equivalent ME effect could be obtained. In PE materials, the mechanical strain and electric field are coupled. In MS materials, the mechanical strain and magnetic field are coupled. By linking two such materials mechanically, the resulting pseudo ME effect can be demonstrated simply as [9]

$$ME Effect = \frac{electrical}{mechanical} \times \frac{mechanical}{magnetic}$$
 (1)

where the mechanical components in essence cancel out. In 1998 Shin et al. attempted a three-layer laminate composite approach where the MS material was sputtered as a thin film onto a glass substrate which was then bonded onto a PE base. This design has become known in the literature as a unimorph. By applying a voltage to the PE, the bending strain induced into the MS material caused large changes to its magnetic properties [10].

Building on the ME laminate approach taken by Shin et al., Ryu et al. developed another ME laminate using a sandwich design. This design used silver epoxy to bond a PZT-5A PE disk between two Terfenol-D MS disks. Measuring the magnetoelectric coefficient under various magnetic field strengths yielded values up to 4.68 V/(cm·Oe) [11]. Not only was this an overwhelming improvement to the magnetoelectric coefficient, it brought the ME effect to a point of usefulness. Following closely on the work done by Ryu et al., Dong et al. published a series of papers which have become seminal works for the design and modeling of sandwich, or extensional bimorph, ME transducer designs and configurations [12–15]. Their work created model subsets for each of the four coupling orientation combinations possible for the PE and MS materials within the laminate structure. These configurations are compiled and shown in Figure 1 and indicate whether the PE and MS materials are poled longitudinally or transversely to the bimorph structure.

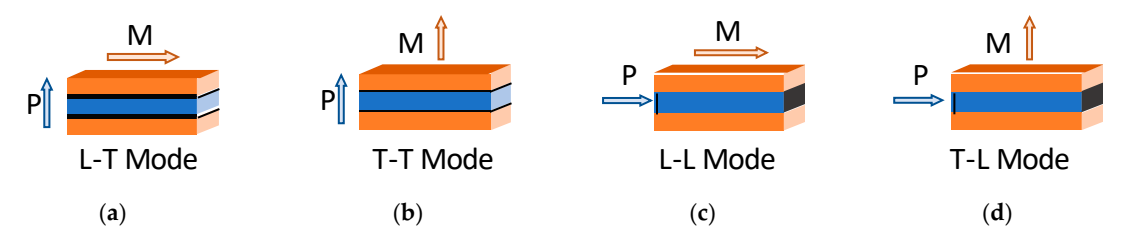


Figure 1. From himorph laminate vicentation combinations. Orange indicates naggatestrictive (MRs) material blue turpice electric (PE) material and black turbection of the Pelectrodes Additionally, thre letters in thremouse names. It for transverse and L for longitudinal indicated breasing transverse and L for longitudinal indicated breasing transverse. Marnaterial pard Primaterial i respective by (a) Lt Mudac (b) Tt Mudac (a) Lt IMudac (d) Tt IMudac. Compiled from [122-15].

Frundlancentally, annugurated leatric transclucer is any device that takes core gryfrom the magnetic dbonaainttottheedectric dhomain and wiee wersa. Recently, anothertyge coffWEtransducer has been proposed. This transducer operates by coupling the moment induced on a ferromagnet by an external maggietic ffeeld with a bending IRE beam. This is done by an an boing one endo of the beam and by mountingtheferromagnetatthetipofilbebeamooidentelberpendiculantothefilield [6] [Talhispoint, most of the research done consuch a device has been for the purpose of energy scavenging and the corresponding models are sparse. Nevertheless the designs blows significan promines to the WIP[16468]. 18ulHidalticationa ha ve y to tusa se comaiste tetra ana écrot blasse con et my. It will be referred to im this work simplyasaMechano-MagnetoelectricorMME device.

Assignificantad/vantageof/magnetoblectrict nanshlucers/forthecuse/in/WPTsystems/fortMDsiss thatfor a given operating frequency, an efficient receiver an bonderer of on again telebrarial at that an fBFTIBIT RF: VRFT VAUSTE mast Ethis. Of this shears so the nedective magnetic avaverted done enternated at the control of the racobatical acobations desired transduced transchuricity to February in Fraquericzen deceptions a valengths vanvehengthmallenthen sheatterntagnetieennomlengthe. Willendgehet Ol Hinsilhengeste dirtilizingset ME uhilizinghafMEransountphefouetponseuntaneales joo2008 t.Thusiterese 2008s Morard eben inhaitha Webutuh'atene inter acoul chareneous tee? cold at a relistance no Warra fristanactranismitting is chemaid in the line is took no the final of O aliasade et a la implada se é é a homa kei relses é ordoscopy, det ess em de sogrands aurei a al doods midist de neglit tbiolandhighusbeone Mi Erbaneth e VIST bi ONIEN baneth e NEST, i 20 y c Ni bheithe e assir i a two ith ithip peace ptian wifts on a c efinetotialencentoracificationalement very flictationas words, done to the characteristical to seasoch functional [24]. researEhararans(21)f. this paper is to critically evaluate ME laminates and MME transducers as candilleteafaposireléstpis yeapereix és initi MPF systèma tionWND an Anatush albe eVANDA tourind apporates cexiditingenedical iadets countraines (22er34).nLanwell element foodAlDfar Aothutypethef systhmiane ideorphopateauxickiperimediallysuuldidatedistraintst [22e24b] dals mopetire lidricated is to be in the control of the control system numerical apprintization experimental ly head that applicated plusially designs an adology portion to a remodule cr chesigns the enchds in the contrict and white i palwaye in the chniques. These two optimal designs are compared to one another and to the needs of theoretical WPT powered IMDs.

- 2. Materials and Methods
- 2. Materials and Methods taken in this work is to develop lumped element models for each type of transduces stabajosto text taxos ducers using off-the abelian aterials acceptainentally evalidate the models this is at the tent transducers transducers is allow optimize the right as microefabricated, version of the nAffetransdugera-using the validate almodalae Thin section will be year the modeline abbrication estiest of the MEStrans diversimental methands ated models. This section will cover the modeling, fabrication of test structures, and experimental methods. 2.1. Lumped Element Model for ME Devices
- 2.1. Lidered Element Molecule Medical Representation 2.1. Lidered Element Medical Representation 2.1. Lidered order of the magnetoelectric voltage coefficient as L-L, L-T, T-L, T-T. In practical terms, the L-L and T-L Dong et al. 914.151 rank the four ME laminate configurations shown in Figure 1 in descending configurations are extremely difficult to tabricate on a small scale. Therefore, the L-T configuration was order of the magnetoelectric voltage coefficient as L-L, L-T, T-L. In practical terms, the L-L and chosen for further consideration. The laminate is considered to be mounted at the center, as shown T-L configurations are extremely difficult to fabricate on a small scale. Therefore, the L-T configuration was chosen for further consideration. The laminate is considered to be mounted at the

center, as shown in Figure 2, making a longitudinal mode resonator. This structure can be modeled by the legit valent circuit shown in Figure 3, making a longitudinal mode resonator. This structure can be modeled by the legit valent circuit shown in Figure 3, which is a slight alteration of the equivalent circuit developed by increase a longitudinal mode resonator. This structure can be modeled by the legit valent circuit shown in Figure 3, which is a slight alteration of the equivalent circuit developed by increase a longitudinal mode resonator. This structure can be modeled by the legit valent circuit shown in Figure 2, making a longitudinal mode resonator. This structure can be modeled by the longitudinal mode resonator. This structure can be modeled by the longitudinal mode resonator. This structure can be modeled by the longitudinal mode resonator. This structure can be modeled by the longitudinal mode resonator. This structure can be modeled by the longitudinal mode resonator. This structure can be modeled by the longitudinal mode resonator. This structure can be modeled by the longitudinal mode resonator. This structure can be modeled by the longitudinal mode resonator. This structure can be modeled by the longitudinal mode resonator. This structure can be modeled by the longitudinal mode resonator. This structure can be modeled by the longitudinal mode resonator. This structure can be modeled by the longitudinal mode resonator. This structure can be modeled by the longitudinal mode resonator. This structure can be modeled by the longitudinal mode resonator. This structure can be modeled by the longitudinal mode resonator. This structure can be modeled by the longitudinal mo optimization of received power added to enable the calculation and optimization of received power.

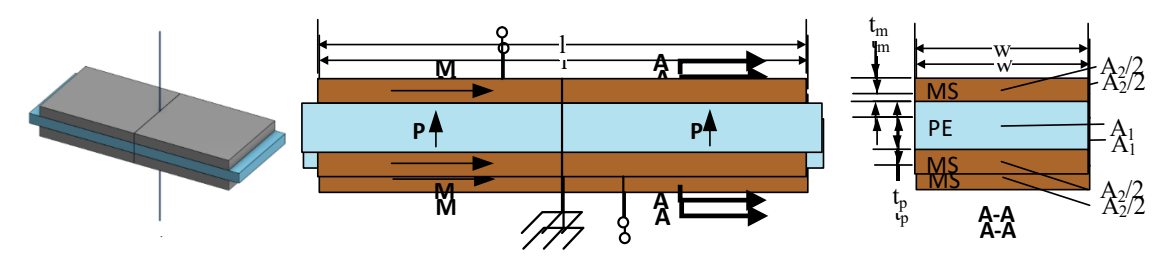


Figure 2. Geometry layout for L-T mode bimorph. Arrows M and P show the magnetization and Figure 3. Geometry, layout for L-T mode bimorph: Arrows M and P show the magnetization and polarization orientation. Adapted from [13]:

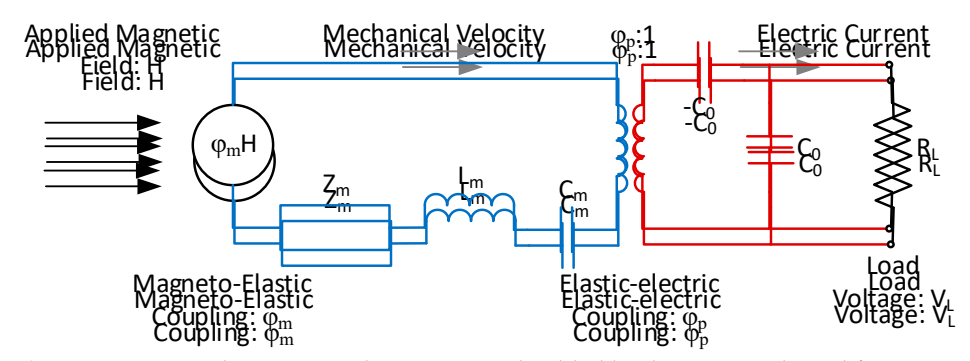


Figure 3. Masnetoelectric equivalent circuit with added load resistor. Adapted from [13]:

As shown in Figure 3, the WS9 transdctitions is modeled by the magnetoelectric coupling factor, As shown in Figure 3, the MS transduction is modeled by the magnetoelectric coupling factor, which is defined as ρ_m , which is defined as

which is defined as $\varphi_m = \frac{A_2 d_{33,m}}{A_2 d_{33,m}} \begin{bmatrix} N \\ A_2 d_{33,m} \\ A_3 d_{33,m} \end{bmatrix}$ where A_2 is the total cross-sectional area of the MS layers, $d_{33,m}$ is the magneto-elastic or piezomagnetic where A_2 is the total cross-sectional area of the LL ayers, $d_{33,m}$ is the magneto-elastic or Whatecoastic entre in the longitudinal direction, and S_{12}^{12} is the elastic compliance of the piezomagnetic (PM) coefficient in the longitudinal direction, and S_{12}^{12} is the elastic compliance of the piezomagnetic (PM) coefficient in the longitudinal direction and S_{12}^{12} is the elastic compliance of the piezomagnetic field level. However, which is the piezostation of the p

$$\varphi_{p} = \frac{v(\mathbf{g}, \mathbf{g}, \mathbf{g}, \mathbf{h}, \mathbf{h})}{\varphi_{p}} \underbrace{\frac{v(\mathbf{g}, \mathbf{g}, \mathbf{g}, \mathbf{h}, \mathbf{h})}{\varphi_{p}} \underbrace{\frac{v(\mathbf{g}, \mathbf{g}, \mathbf{g}, \mathbf{h}, \mathbf{h})}{\varphi_{p}}} \underbrace{\frac{v(\mathbf{g}, \mathbf{g}, \mathbf{g}, \mathbf{h}, \mathbf{h})}{\varphi_{p}}} \underbrace{\frac{v(\mathbf{g}, \mathbf{g}, \mathbf{g}, \mathbf{h}, \mathbf{h})}{\varphi_{p}}} \underbrace{\frac{v(\mathbf{g}, \mathbf{g}, \mathbf{g}, \mathbf{h}, \mathbf{h}, \mathbf{h})}{\varphi_{p}}} \underbrace{\frac{v(\mathbf{g}, \mathbf{g}, \mathbf{g}, \mathbf{h}, \mathbf{h}, \mathbf{h}, \mathbf{h})}{\varphi_{p}}} \underbrace{\frac{v(\mathbf{g}, \mathbf{g}, \mathbf{g}, \mathbf{h}, \mathbf{h$$

where wand draff the width and length of laminates the interthickness of the piezoelectric layers as the teams of the piezoelectric layers are the teams of the piezoelectric contains conflict the language of the piezoelectric contains and the language of the piezoelectric layers and the language of the layers and the layers are large of the layers and the layers are layers and layers are layers are layers and layers are layers are layers and layers are layers are layers layer The electrical capacitance in the circuit, C_0 , is the clamped capacitance of the piezoelectric material, and if the electrical capacitance in the circuit, C_0 , is the clamped capacitance of the piezoelectric material, and is defined as $C_0 = \frac{wl}{l} \frac{N}{V}$ (4)

The value for $\overline{\beta}_p$, the effective inverse dielectric point ant, is calculated by The value for $\overline{\beta}_p$, the effective inverse dielectric point ant, is calculated by $\{4\}$

The value for $\overline{\beta}_{p'}$, the effective inverse dielectric constant, is calculated by $\overline{\beta}_{p} = \beta_{p} \left(1 + \frac{831}{s_{11}^{D}\beta_{p}}\right) \left[\frac{m}{F}\right]$

$$\overline{\beta}_{p} = \beta_{p} \left(1 + \frac{8\overline{31}}{s_{11}^{D}\beta_{p}} \right) \left[\frac{m}{F} \right]$$
 (5)

Materials **2019**, 12, 512 5 of 18

The mechanical damping coefficient, Z_m , inductance (inertia), L_m , and capacitance (compliance), C_m are defined as

$$Z_m = \frac{\pi Z_0}{4Q_m} \left[\frac{kg}{s} \right] \tag{6}$$

$$L_m = \frac{\pi Z_0}{4\omega_s} \left[kg \right] \tag{7}$$

$$C_m = \frac{1}{\omega_s^2 L_m} \left[\frac{s^2}{kg} \right] \tag{8}$$

where Q_m is the effective mechanical quality factor for the laminate, ω_s is the fundamental frequency of the laminate, and Z_0 is the characteristic mechanical impedance of the laminate in the extensional model. These remaining lumped mechanical parameters were derived by Dong et al. [15] by solving the second order equation of motion for the system. The results of this derivation are summarized in Table 1.

Table 1. Lumped parameter equations for L-L magnetoelectric (ME) laminate. Adapted from [15].

Lumped Parameter Variable	Constitutive Equation			
Characteristic Mechanical Impedance, Z_0	$Z_0 = \rho_{avg}v * (A_1 + A_2) \left\lceil \frac{\text{kg}}{\text{s}} \right\rceil$			
Average Laminate Density, $ ho_{avg}$	$Z_0 = ho_{avg}v*(A_1+A_2)\left[rac{\mathrm{kg}}{\mathrm{s}} ight] \ ho_{avg} = rac{ ho_{ms}A_2 + ho_{me}A_1}{A_1 + A_2}\left[rac{\mathrm{kg}}{\mathrm{m}^3} ight]$			
Magnetoelectric Wave Speed, $\it v$	$v=\sqrt{rac{n}{s_{33}^H}+rac{(1-n)}{s_{13}^D}}\left[rac{ ext{m}}{ ext{s}} ight]$			
Volumetric Layer Ratio, n	$n = \frac{A_2}{A_2 + A_1}$			
Fundamental Frequency, $\omega_{\scriptscriptstyle S}$	$\omega_s = rac{\pi v}{l} \left[rac{rad}{s} ight]$			
Effective Laminate Quality Factor, Q_m	$Q_m = \left(rac{n}{Q_{ms}} + rac{1-n}{Q_{me}} ight)^{-1}$			
Magnetostrictive Material Density, ρ_{ms}	Material property			
Piezoelectric Material Density, ρ_{pe}	Material property			
Magnetostrictive Quality Factor, Q_{ms}	Material property			
Piezoelectric Quality Factor, Q_{pe}	Material property			

A frequency domain circuit analysis on the equivalent circuit of Figure 3 yields the following expression for the effective ME coefficient,

$$\alpha_{me} = \frac{\partial V_L}{\partial H} = \left| \beta \frac{\varphi_p}{j\omega C_0 + \frac{1}{R_L}} \frac{\varphi_m}{Z_m + j\omega L_m + \frac{1}{j\omega C_m} + \varphi_p^2 Z'} \right| \left[\frac{V}{A/m} \right]$$
(9)

where $\beta \leq 1$ is the ME bias factor, which will be discussed in more depth in the following section, ω is the operating frequency of the magnetic field H, and Z' is the impedance of the electrical portion of the circuit of Figure 3 given by

$$Z' = \frac{R_L}{j\omega C_0 R_L + 1} - j\omega C_0[\Omega] \tag{10}$$

One will note that the piezoelectric coupling factor, φ_p in Equation (9), is not squared as it is in [15]. It appears that this is an error in the reporting of the original model in [15].

The zero-peak load voltage (V_L) can then be calculated by

$$V_L = H_p |\alpha_{me}| [V] \tag{11}$$

where H_p is the magnitude of the sinusoidal magnetic field. Finally, the RMS power (P_{RMS}) is calculated as

$$P_{RMS} = \frac{1}{2} \frac{V_L^2}{R_L} [W] \tag{12}$$

$$V_L = H_p |\alpha_{me}| [V] \tag{11}$$

where H_p is the magnitude of the sinusoidal magnetic field. Finally, the RMS power (P_{RMS}) is calculated as

Materials 2019, 12, 512
$$P_{RMS} = \frac{1}{2} \frac{V_L^2}{R_L} [W]$$
 6 (12)

This model makes a few assumptions that need to be made explicit. First, the model assumes complete and uniform strain transfer from the layer layer layer. Taxe in this implies that the fact interface joint between the laminates is infinitely fait there is no strain the dignt the much the joint between the laminates is infinitely fait there is no strain the dignt the much the brightness of the same the laminates is infinitely fait there is no strain the properties of the prop

$$d_{33m} = \frac{d\lambda_{d\lambda}}{dH} \tag{13}$$

where λ is the magnetostriction of a given MS material [25]. Simply put, the PM coefficient is the rate where λ is the magnetostriction of a given MS material [25]. Simply put, the PM coefficient is the of change of magnetostriction with respect to magnetic field. As indicated by Figure 4 magnetostriction with respect to magnetic field. As indicated by Figure 4 is nonlinear and furthermore d_{33} is quite low at or near zero magnetic field. An effective transducer magnetostriction is nonlinear and furthermore d_{33} is at a maximum, which requires that the MS material be biased, effective transducer will operate near a point where d_{33} is at a maximum, which requires that the MS material be biased. Effective transducer will operate near a point where d_{33} is at a maximum, which requires that the MS material be biased. Biasing is done by applying a direct current (DC) magnetic field (H_{DC}) to effectively move the ME maximum point to the maximum piezomagnetic coefficient value. To account for the DC effectively move the ME, laminate operating point to the maximum piezomagnetic field bias, which varies fremendously by material, Dong et al. added the variable β to account for the DC magnetic field bias, which varies tremendously by material, Dong et al. added the variable β to equation β . A value of β = 1 means the structure is optimally biased; a value of β = 0 means the tructure is not biased at all. [15]. This component of the model has to be evaluated experimentally as β = 0 means the structure is not biased at all. [15]. This component of the model has to be evaluated experimentally as the optimal bias varies by geometry, material selection, and mechanical preload. Work has been done experimentally as the optimal bias varies by geometry, material selection, and mechanical preload. Work has been done to build self-biased ME structures that eliminate the need for biasing, however, that research is still premature and beyond the scope of this work [26].

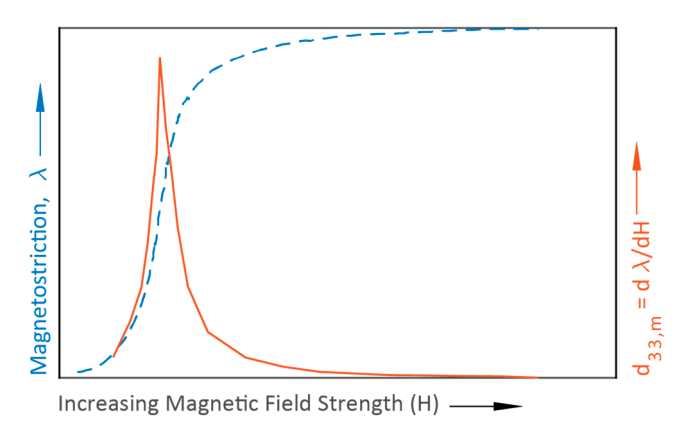
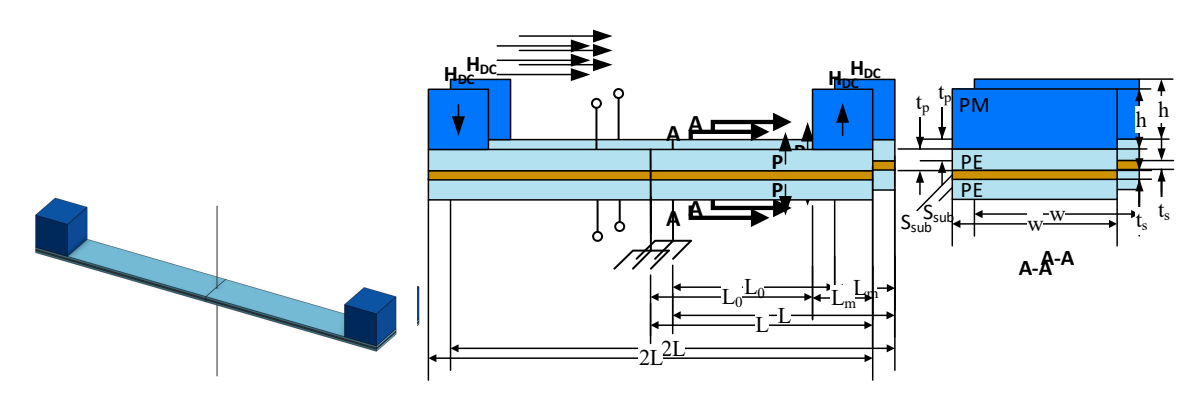


Figure 4. A typical magnetostriction profile and its derivative. Adapted from [25].

2.2. Lumped Element Model for MME Devices

Figure 5 shows a MME device. The device utilizes a single piezoelectric bending laminate composed of a PE top layer, a structural center layer (Saub), and another symmetric PE bottom layer. Strain is induced on the structure by anchoring the bending laminate at the center and adding oppositely oriented permanent magnetical its ends. When a magnetic field is applied along the length of the structure, the beam experiences a pure bending moment.



Figures 5. Compared Algorical and the claudia contiler of the continuous section of the continuous A Action is marked to indicate PE making alterations and acrow an inchest the minding the priminated out the there mannent magnetic fields.

THE BEAR WIND A CONTROL OF THE BEAR OF THE carapt bessernt hat the countest is further mentally is similar to the MT Lamine at convolet hands blazens the same parameneters funt le prizieze ettert i ganation un the crimuit.

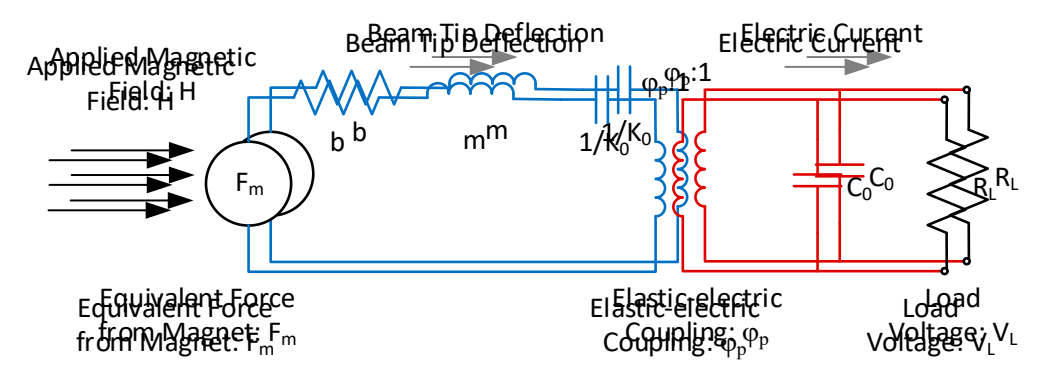


Figure 6. Equivalent circuit model of a double cantilever MME structure.

THE POWER OUTPUT OF THE MAN TEST HICKORY IS CALCULATED AS

$$P_{P}^{\underline{P}} = \frac{1}{2} \frac{1}{2} \underbrace{\frac{1}{2} \frac{K}{M} \frac{\omega u_{2}^{2} \tau}{\frac{1}{2} \frac{1}{2} \frac{\omega u_{2}^{2} \tau}{M}} \underbrace{\frac{1}{2} \frac{1}{2} \frac{1$$

wwwhere where

$$\tau_{\overline{t}} = R_{C} G_{S}[S], \qquad (15)5)$$

$$\Delta A = \frac{g_{\text{tot}}^2 \sqrt{N}}{C_{\text{tot}}^2 \sqrt{N}}, \qquad (16)99)$$

$$\mathcal{L}_{p} = \frac{4e_{1}e_{2}w_{1}w_{1}e_{1}e_{1}+\frac{1}{2}\sqrt{3M_{1}+m_{1}}\sqrt{32-3m_{1}}\sqrt{4e_{1}+m_{1}}\sqrt{3e_{1}}\sqrt{1+m_{1}}\sqrt{3e_{1}}}{66M_{1}+m_{1}}\sqrt{3e_{1}+m_{1}}\sqrt$$

andand

$$|X_0|^2 = \frac{F_0^2}{|X_0|^2} [m^2]$$

$$|X_0|^2 = \frac{|X_0|^2}{|X_0|^2} = \frac{|X_0|^2}{|X_0|^2} \frac{|X_0|^2}{|X_0$$

At optimal load resistance and ope statedsas

At optimal load resistance and open-circuit resonance frequency, the optimal average power is stated partial load resistance and open-circuit resonance frequency, the optimal average power is stated as
$$P_{AVG}^{opt} = \frac{F_0}{4h} M_1 \left(\sqrt{M_1^2 + 1} - M_1 \right) [W]$$

$$P_{AVG}^{opt} = \frac{F_0 F_0}{4h} M_1 \left(\sqrt{M_1^2 + 1} - M_1 \right) [W]$$

$$P_{AVG}^{opt} = \frac{F_0 F_0}{4h} M_1 \left(\sqrt{M_1^2 + 1} - M_1 \right) [W]$$

$$(16)^9)$$

Materials 2019, 12, 512 8 of 18

where

$$M_1 = \frac{\Delta K}{b\omega_1} \tag{20}$$

In this case, the optimal load resistance is calculated as

$$R_L^{opt} = \frac{\sqrt{M_1^2 + 1}}{\omega_{1C_0}} [\Omega] \tag{21}$$

For the sake of simplicity, the variables and constitutive equations that compose Equations (14)–(21) are summarized in Table 2. One can note that the model for the MME is significantly more convenient than the ME model because there is a closed-form solution for the optimal load and power. A full derivation of Equations (14) though (21) is found in [18]. (Note that unlike [18], Figure 5 neglects the finite length of the center clamp. However, this has no effect on the generality of the model.).

Lumped Parameter Variable Constitutive Equation

Table 2. Lumped parameters for MME transducer.

bean Lengui, L	Differsion		
Beam Length up to Magnet, L_0	Dimension		
Beam Substrate Thickness, t_s	Dimension		
PE Layer Thickness, t_p	Dimension		
Magnet Mass, M	$M = \rho_M V_M [kg]$		
Magnet Mass, M	$M = \rho_M V_m [kg]$		
Beam Mass, m_b	$m_b = \rho_s V_s + \rho_{PE} V_{PE} [kg]$		
Equivalent Mass, m	$m=M+rac{33}{140}m_b$ [m]		
Equivalent Moment Force, F_m	$F_M = \frac{3M_b}{2I_{eff}}[N]$		
Short-circuit Stiffness, K_0	$K_0 = \frac{3(YI)_c}{l_{eff}^3} \left[\frac{N}{m} \right]$		
Open-circuit Stiffness	$K_1 = K_0 + \Delta K \left[\frac{N}{m} \right]$		
Piezoelectric Capacitance, C_0	$C_0 = \frac{wL}{t_p\beta_p} [F]$		
Open-circuit resonance Frequency, ω_1	$C_0 = \frac{wL}{t_p\beta_p} \begin{bmatrix} E \end{bmatrix}$ $\omega_1 = \sqrt{\frac{K_1}{m}} \begin{bmatrix} \frac{\text{rad}}{s} \end{bmatrix}$		

2.3. Fabrication of Test Structures

Two ME transducers were built to validate the model. Two material structure combinations were built: a Galfenol and lead zirconate titanate (PZT) laminate and a Metglas 2605SA1 (Metglas[®] Inc., Conway, SC, USA) and polyvinylidene fluoride (PVDF) laminate. Terfenol-D was avoided due to the difficulties associated with machining a brittle, pyrophoric material.

To build the Galfenol-PZT device, 25.4 mm diameter TdVib Galfenol (TdVib LLC, Ames, IA, USA) was cut using electrical discharge machining into two 10 mm \times 20 mm \times 370 μ m sheets poled along the 20 mm length. The PE material used was 1.02 mm thick Piezo Systems PZT-5A (T140-A4E-602, Piezo.com, Division of Mide Technology, Woburn, MA, USA) which was cut using a diamond blade dicing saw to a single 10 mm \times 20 mm sheet poled through the thickness. The three layers were then bonded together such that the PE layer was sandwiched between the ME layers. EPO-TEK H20S silver filled (conductive) epoxy was used to adhere the laminate. The epoxy was cured using a heat press, following the epoxy's minimum cure instructions. Finally, two 0.635 mm right angle header pins were bonded to the top and bottom Galfenol. This bond was done using MG Chemicals silver conductive epoxy given that the joint wasn't structural. This epoxy was cured overnight at room temperature. The resulting transducer can be seen in Figure 7a.

heat press at the minimum prescribed cure. Similar leads were also bonded as before, however this time on the center flange of the PVDF. The final structure can be seen in Figure 7b.

The MME device was constructed from an of off-the-shelf PZT4A bimorph from Piezo Systems Inc. with overall dimensions of $32.55 \times 3.175 \times 0.38$ mm. Two Neodymium magnet cubes of 3.175 mm Material PMGP where bonded to the ends of the PZT beam with cyanoacrylate. The final structure 18 shown in Figure 7c.

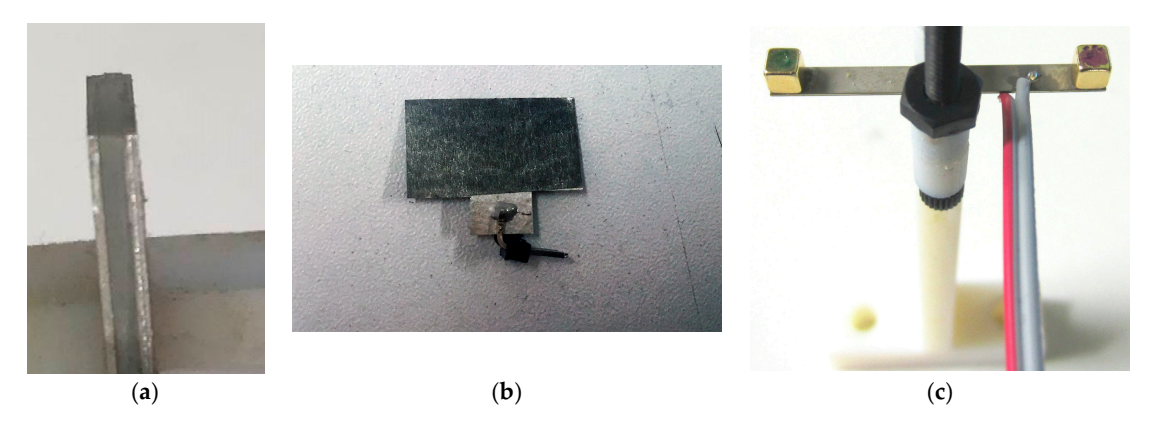


Figure 7. Images of abbirated decess tructures s.a. (Soldan chord zir zonata ditaneta de ZOZO) inata de. (Boldan chord zir zonata ditaneta de ZOZO) inata de. (Boldan chord zir zonata de LOZO) zir inata de. (Boldan chord zir zonata de LOZO) zir inata de. (Boldan chord zir zonata de LOZO) zir inata de. (Boldan chord zir zonata de LOZO) zir inata de.

2.4. Experimental Publis device was built in a fashion similar to that of the Galfenol-PZT device. Raw 23 µm thick 2605SA1 Metglas was cut using scissors into two 10 mm × 20 mm layers. The In order to characterize the ME and MME transducers, a nested Helmholtz coil was constructed nature of amorphous Metglas is such that magnetostriction occurs at any orientation in the sheet to create a uniform alternating current (AC) magnetic field superimposed on a DC magnetic field. By plane so poling direction was unimportant. To match the very thin Metglas, metalized PVDF (TE superimposing the two fields, ME transducers could be both biased with the DC field and driven 1-1004347-0) was used. These sheets themselves were a sandwich of 28 µm PVDF with 6 µm silver with the AC field. (Note that the MME transducer does not need a DC biasing field.) The system ink electrodes on the top and the bottom, poled through the thickness. These sheets were also cut diagram for this setup and the nested Helmholtz coil are shown in Figure 8. to 10 mm × 20 mm; however, a small tab was left so that electrical leads could be attached to the PE while using a non-conductive epoxy. In particular the nonconductive epoxy EPO-TEK H70E was used for its slightly hinner minimum bond line of less than 20 µm compared to the silver filled alternative which was measured on the Galfenol-PZT device to be about 35 µm. As before, the epoxy was cured in a heat press at the minimum prescribed cure. Similar leads were also bonded as before, however this time on the center flange of the PVDE The final structure can be seen in Figure 70.

The MME device was considered from an of off-the-shelf PZT A bimorph from Piezo Systems Inc. with overall dimensions of the PZT beam with cyanoacrylate. The final structure is shown in FQsqilles cope

Transducer Voltage R_L Nested
Helmholtz Coil

In order to characterize the ME and MME transducers, a nested Helmholtz coil was constructed to create a uniform alternating current (AC) magnetic field superimposed on a DC magnetic field. By superimposing the two fields, ME transducers could be both biased with the DC field and driven with the AC field. (Note that the MME transducer does not need a DC biasing field.). The system diagram for this setup and the nested Helmholtz coil are shown in Figure 8.

The nested Helmholtz coil can deliver an AC magnetic field (H_p) of 2-Oe (2 G in air) at 150 kHz with a 40-watt, 50 Ω amplifier (E&I 240L, Rochester, NY, USA) with no additional circuitry (i.e., tuned resonating capacitors) and a DC magnetic field (H_{DC}) of 16-Oe without exceeding the safe wire gauge current. The uniformity of the field was measured using an AlphaLab UHS2 gaussmeter. The AC coil was measured to have 2% field variation over ± 1.5 cm at the coil origin (the point co-linear to the coil axis and equidistant from the inner coil faces) along the axial center line. The DC coil had less than 5% variation over the same length. For this and all other work the AC coil was driven by a Tektronix AFG1022 signal generator (Tektronix Inc., Beaverton, OR, USA) and either an E&I 240L (E&I, Rochester, NY, USA) or a Rigol PA1011 amplifier (Rigol Technologies Inc., Beaverton, OR, USA). The DC coils were driven with a B&K Precision 9201 power supply (B&K Precision Corporation, Yorba Linda, CA, USA).

2.4. Experimental Methods

In order to characterize the ME and MME transducers, a nested Helmholtz coil was constructed to create a uniform alternating current (AC) magnetic field superimposed on a DC magnetic field. By superimposing the two fields, ME transducers could be both biased with the DC field and driven which and the MME transducer does not need a DC biasing field.) The system diagram for this setup and the nested Helmholtz coil are shown in Figure 8.

The nested Helmholtz coil can deliver an AC magnetic field (H_D) of 2+Oe (2 G M Ray at 150 kHz with a 40-watt, 50 Ω amplifier (H&I 240L, Rochester, NY, USA) with no additional circliffy (i.e., tuned resonating capacitors) and a periodic field (H_{DC}) of 16-Oe without exceeding the safe wire gauge current. The uniformity of the field was measured using an AlphaLab UHS2 gaussmeter. The AC coil was measured to have 2% field variation over ±1.5 cm at the coil origin (the point co-linear to the coil axis and equicilists upper om the inner coil faces) along the axial center line. The DC coil had less than 5% variation over the same length. For this and all otherwork the AC coil was driven by a Tektronix AFG1022 signal generator (Tektronix Inc., Beaverton, OR, USA) and either an E&C 240L (E&I, Rochester, NY, USA) or a Rigol PA1011 amplifier (Rigol Technologies Inc., Beaverton, OR, USA). The DC coils were driving the same length of the line of the language of the same length of the line of the language of the lan

The BE soil is sufficient to optimally bias the Metglas-PVDF ME structure. However, it is not sufficient to bias the Calcend-PZT ME structure which requires a bias included 1900 of Poe. Therefore, accordingly or or an analysis in the calcendate of the structure which requires a bias included 1900 of Poe. Therefore, accordingly or or or of the distance of the calcendate of the or of the calcendate of the c

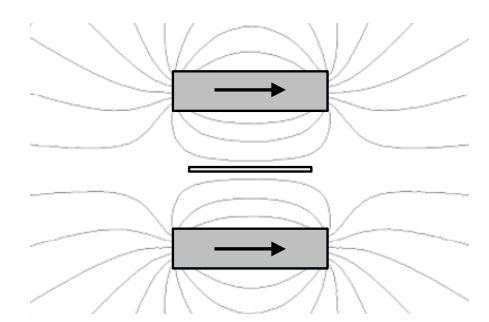


Figure 9: Biasing magnet arrangement and resulting field lines: Transducer is shown in between the two magnets:

The following three basic steps were performed to characterize the ME and MME devices and validate the lumped element models: optimize magnetic field bias, measure open circuit voltage as a function of frequency and magnetic field, measure power delivered to an optimized resistive load.

To determine the optimal field is a force and international and field is a force and the device and an international applies the device and t

Open circuit measurements were performed by sweeping the frequency of the magnetic field from 50 to 150 kHz at a state of 212.15 Hz/sz/10 cross distribution). The field amplitude was set at $H_{1p} \equiv 1.0$ centrol kHz, however this value attenuated as the sweep progressed due to the increasing coil impedance. To compensate, the magnetic field level and open circuit transducer voltage were measured simultaneously and then normalized for all of the sweeps performed. The normalization was done by performing an FFT on the signals then dividing the resulting transducer voltage amplitude by the field amplitude. The result was then multiplied by $H_{RMS} = 0.707$. Oe to find the open circuit RMS voltage, V_{ORMS} , across the sweep frequency. It should be noted that this

coil impedance. To compensate, the magnetic field level and open circuit transducer voltage were measured simultaneously and then normalized for all of the sweeps performed. The normalization was done by performing an FFT on the signals then dividing the resulting transducer voltage amplitude by the field amplitude. The result was then multiplied by $H_{RMS}=0.707$ Oe to find the open circuit RMS RMS, RMS, RMS RM

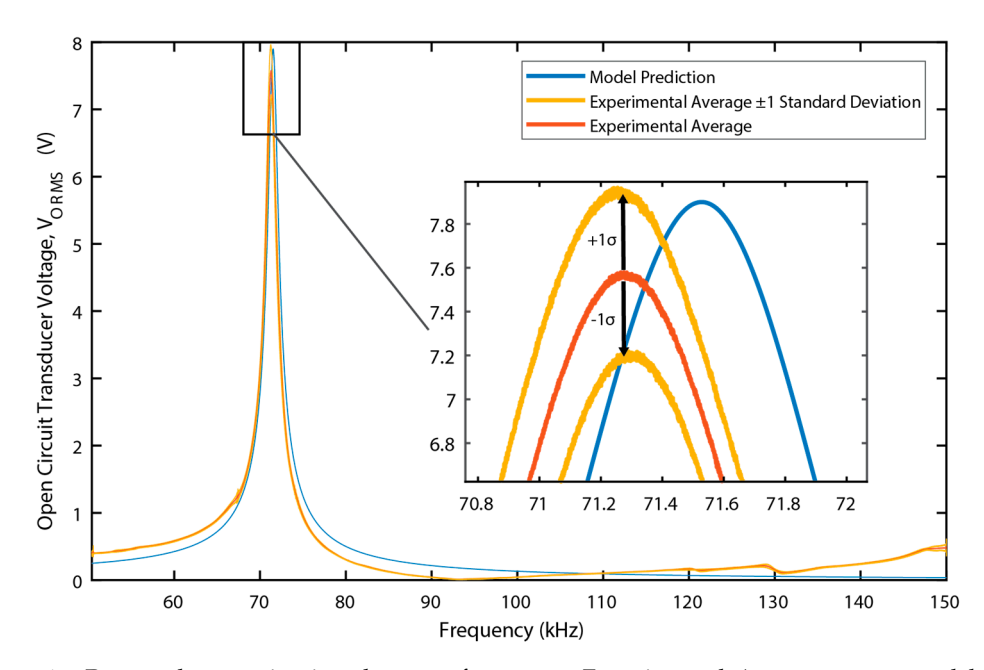


Figure 10. Repeated open circuit voltage vs frequency. Experimental Average, upper and lower deviation, and model prediction shown:

Once the resonance frequency was determined, the wolltage output was measured across a load resistor to determine the thougo generated Ted. loaderesistance is tance experimental pedetermally the optimal heads Time generated powerated power to be taken ower dissipated at the original had privited load in This procedular in the optimal had privited load in the original transcept and the three depicts of the original transcent in the original pedetermined the original transcent in the

3. Results

A primary goal of this work is to rigorously compare different magnetoelectric transducer architectures for use as wireless power receivers for biomedical implants That approach taken is tedevolop ratelel foloecach architecture, experimentally validate those models using off the shelf materials, and then use the models to optimize and compare each architecture within the constraints of a biomedical implant. This section contains both the experimental results that validate the models and the results of the constrained optimization procedure to compare each architecture.

3.1. Model Validation Results

The measured and simulated open circuit voltage as a function of frequency for the Metglas-PVDF device is shown in Figure 11. (The open circuit voltage for the Galfenol-PZT device is shown above in Figure 10) In both cases, the DC magnetic field was optimally biased prior to the measurements. In the case of the galfenol-PZT device, both the measured voltage magnitude and resonance frequency match the simulation very closely. In the case of the Metglas-PVDF device, the

3.1. Model Validation Results

The measured and simulated open circuit voltage as a function of frequency for the Metglas-PVDF device is shown in Figure 11. (The open circuit voltage for the Galfenol-PZT device is shown above in Figure 10) In both cases, the DC magnetic field was optimally biased prior to the measurements. In the case of the galfenol-PZT device, both the measured voltage magnitude and resonance frequency match the simulation very closely. In the case of the Metglas-PVDF device, the measured peak output voltage is approximately 3% below the simulated value and the measured resonance frequency is approximately 8% higher than the predicted value. For this device, the epoxy layers between device Materials 2018, 11 x FOR PEER REVIEW structural layers is a significant fraction (20–35%) of the total laminate thickness. The model does not account for the stiffness and inertial effects of the epoxy layers. The model does not account for the stiffness and inertial effects of the epoxy layers. The strain transfer between layers which will introduce some errors given the relative thickness of the model also assumes perfect strain transfer between layers which will introduce some errors given the relative thickness of the epoxy layers. The model also assumes perfect strain transfer between layers which will introduce some errors given the relative thickness of the epoxy layers.

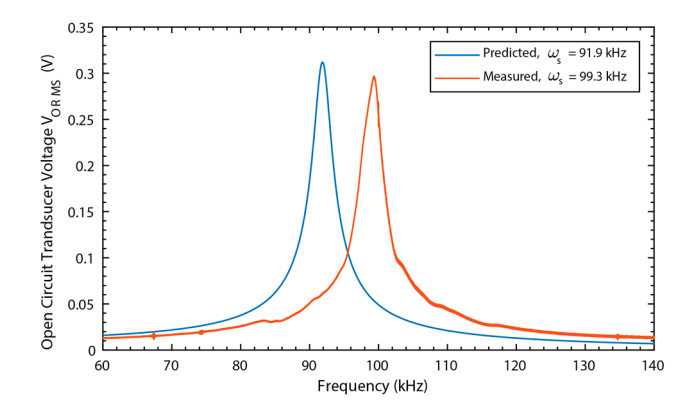


Figure 11: Metglas-PVDF open circuit voltage vs. frequency.

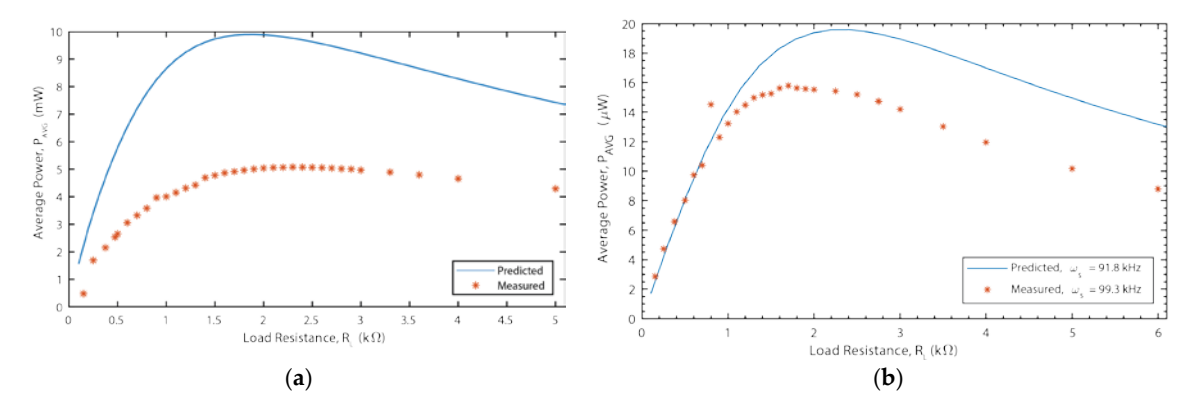
Figure 12 shows the simulated and measured power output for the two ME devices versus load resistance at resonance. Cliently, the discrepancy beterace the model and devices curcinases sehertishe the sististical inadisculfur both Mildericate House van the discrepancy is the particular discrepancy of 50% of 50% after the galfentle galfer load in a discrepancy of the Motellae-Metglad environt particular training and the training and individual since the particular particular training and individual since the particular particular training and individual since the object of the three devices of the that the training and its less uniform and less precisely controlled. Also, the effect of the mechanical mounting clamp will be different for the two devices. Further investigation and refinement in the experimental system is necessary to further investigate this discrepancy. Nonetheless, the model predicts the basic trends and there are reasonable explanations for the discrepancy. Therefore, it was felt that the model was sufficient to be used in a comparative optimization study.

Figure 13, which is reproduced with permission from [18], shows the power output of the MME device as a function of both frequency and AC magnetic field. In the case of the MME device, the equivalent circuit model matches the experimental output very closely. Given the fact that the MME device does not require a DC magnetic field bias and therefore is not affected by the strong nonlinearity in the voltage coefficient with respect to that bias hor the non-uniformity of that bias, this better agreement with experimental results is expected.

Figure 12. (a) Power output vs. load resistance for Galfenol-PZT device operating at 70.7 kHz. (b) Power output vs. load resistance for Metglas-PVDF device operating at 99.3 kHz.

Figure 13, which is reproduced with permission from [18], shows the power output of the MME device as a function of both frequency and AC magnetic field. In the case of the MME device, the equivalent circuit model matches the experimental output very closely. Given the fact that the MME

the bias field is less uniform and less precisely controlled. Also, the effect of the mechanical mounting clamp will be different for the two devices. Further investigation and refinement in the experimental system is necessary to further investigate this discrepancy. Nonetheless, the model predicts the basic trends and there are reasonable explanations for the discrepancy. Therefore, it was felt that the model was sufficient to be used in a comparative optimization study.



Higgure 112. (a) Power output vs. lokal derestance of of a Helical DIZIZ Testievice epatinging 70.7 (kHkHb) (B) Rowen uput put vls. ald adsietastance of McMglts IRVDAD Testievice populinting 89.99 kHkHz.

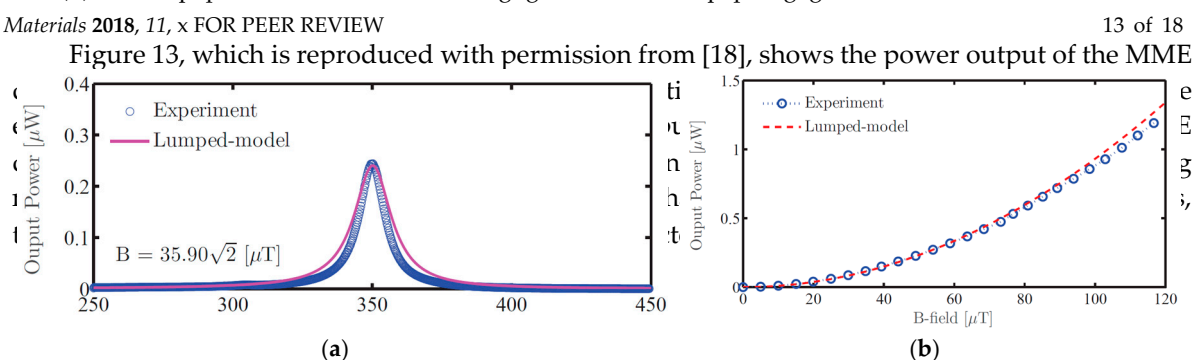


Figure 13: (a) a Exercimental and modeled MMM temperature or year well to the objective field at 350 Hz operating frequency. (Reproduced from [18]), with permission from @ 2018 10P Publishing.).

3.2. Comparative Analysis Results

Three basic types of constraints were placed on the optimization: volume, AC magnetic field amplitude, and geometric constraints to ensure manufacturability. The overall device volume was limited to 2 mm³. This constraint may seem somewhat arbitrary, but is meant to ensure applicability for minimally traumatic IMDs. The exact value of this constraint does not actually significantly alter the comparison results as long as the maximum size is on the order of 1-10 cubic millimeters. The maximum allowable magnetic field was determined using the IEEE standard on magnetic maximum permissible exposure (MIII) for the diseatand to recondere consolute a review mental sonditions (\$222). 1281, that International Gamoinsians non Non Non-Zing Radiantero rection to HCNDR product and and om xianimusc upedioand axpexpus to emegnetic field field. [24] du hath otandarde ahtspline allowable MPIES by tropyroguence to who will be require 17. Terk CICINIR promoted as secondally more conservative than the IEEE standard. Optimizations were performed separately using each standard. Finally, in most cases geometry constraints were coded as aspect ratio constraints to ensure reasonable device geometries for manufacture. A maximum aspect ratio of limit of 200:1 was set for the ratio of beam length (lb) to total debourthicknessess) and for the orative or about the light of aspectraticalipait of the limited the immera aspectratical fluxed for for for the sation the anilong the flux tengidth ()v)o haden (whe in sleebtha ben houted the aspect out itse visible refer to the the interest not the widtle structure width. However, the aspect ratios' length, l_0 does not refer to the total structure length, but the length from both transducers' center anchors to the free edges. This means for the ME transducer $l_0 = 0.5l$ and for the MME transducer $l_0 = L$. Like the maximum volume constraint, these values are somewhat arbitrary based on the authors' own experience. However, they do serve to keep device dimensions to values that could be manufactured and provide a reasonable basis for

However, the aspect ratios' length, l_0 does not refer to the total structure length, but the length from both transducers' center anchors to the free edges. This means for the ME transducer $l_0 = 0.5l$ and for the MME transducer $l_0 = L$. Like the maximum volume constraint, these values are somewhat arbitrary based on the authors' own experience. However, they do serve to keep device dimensions to values that could be manufactured and provide a reasonable basis for comparison of architectures.

Materials 2018, 11, x FOR PEER REVIEW

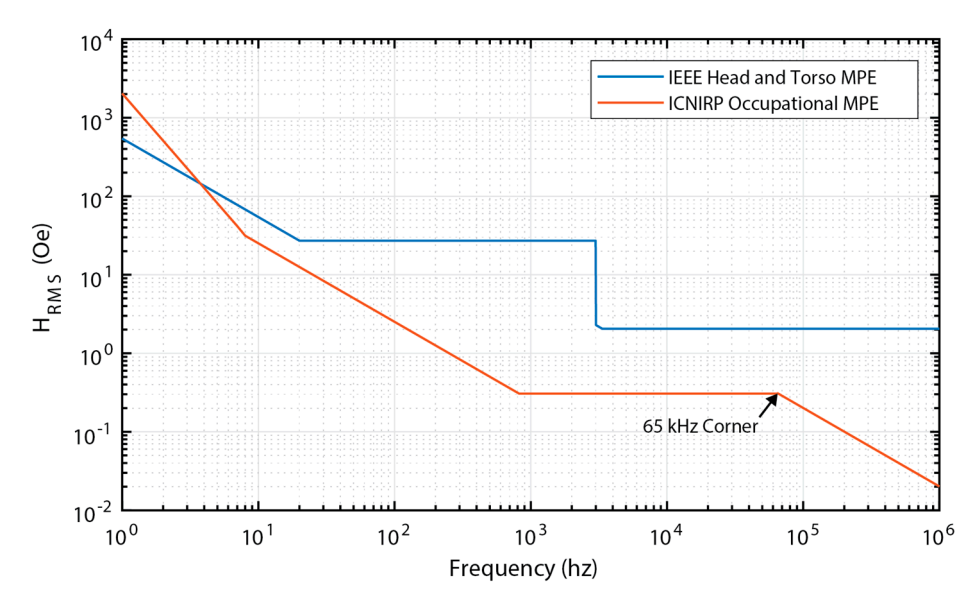


Figure 14: Allowable magnetic MPE levels for IEEE and ICNIRP standards. Adapted from [22=24].

For the MID/He view ion londy maniminimition it in it it is it is the MID/He view ion londy maniminimition it in it is it is the MID/He view ion londy maniminimition it is it is the MID/He view ion londy maniminimition it is it is a constant. Whe) readen a for it could be a first the street of the country and the street of th bepamathlebethenshemelingen offen ageithdeessatten hangt Fifthleyniodebads beesuteet the texte exitimalization ad wraifs nandoutes res fear bestir fater to tallock INAS subject to be the Bear best feature of the control tallock INAS subject to the c gétpikugelektiscasnatapitilor Abthologilctivia anatheratraba ikhacahont foraction bugip than thitatinen stof chou PE relitebility/Titedspescificowaldee ab 100 indiverse determinism du through ficilible exponent strubiley, a practical upper bounFoofthenMMadeplacedooly, the minimum thinkines 1(4) was placed on the ratio of the magnet length (L_m) Table AFE legitifith (Aplic) if the deposition of the one of the breaking stars are calculated and the decision of the L_m treatith, (tw), IREa thi tokund in a tip), NAS third knoses (tag) doached Finat II yal if stepud il dye (av) tead dil lata thees istian izea (tag). Thwaysnahousesconsfigstratiothsickness(pg) of izeds Galfeing-PZT the deMatiglasePZT plsing dhentiately inf piezoeiltietsishovateriiaTaAlekoughdtAisTilma yreothaeribel oposli tyráatitaal (Qyp)eanestatitionatvæhosavoé 48 jindhilitty, watotsepavoragead the aheastheed experimental validies p Each of that ly at jora via a perform tool under 5 hnea different agenthic finelgheunt strakinesst (he). ICNRIP standard, the IEEE standard, and a baseline magnetic field That ME peak naizatiy if requests of the descent short on the standard peak naization is the standard of the That ME peak naizatiy if request of the descent That ME is the standard of the That ME in the standard of the That ME is the standard of t (w), PE thickness (t_n) , MS thickness (t_n) loaded natural frequency (ω) , and load resistance (R_l) . Two material configurations were described in the configuration of the material properties shown it Tables 3 and 4 the mechanical quality factor (Q_m) was set to q value of 48, which was the average of the measured experimental values Fach optimization was performed under three different magneticeleconstraints cherically istandard, the IEEE standard, and mouseline magnetic field of 1 Oe peak at any frequency ρ_{vv} he results of the optimization are shown son Table 18.

Piezoelectric compliance, $s_{11,p}$ 15 × 10 ⁻¹² m ² /N			
Relative Dielectric constant, K_3^T or $(1/(\beta_p \epsilon_0))$	1800		
TdVib Galfenol			
Piezomagnetic coefficient, $d_{33,m}$	15–30 nm/A (15 used)		
Density, ρ_{ms}	7800 kg/m		
Magnetostrictive compliance, s_{33}^H	$12.5-25.0 \times 10^{-12} \text{ m}^2/\text{N} \text{ (16.7 used)}$		

Table 4. Material properties used for Metglas-PVDF model [25,29].

Property	Value	
TE Metallized PVDF		
Piezoelectric voltage coefficient, $g_{31,p}$	$216 \times 10^{-3} \text{ Vm/N}$	
Density, ρ_{pe}	1780 kg/m^3	

Table 3. Material properties used for Galfenol-PZT laminate model.

Property	Value			
Piezo Systems PZT-5A4E				
Piezoelectric voltage coefficient, g _{31,p}	$-11.6 \times 10^{-3} \text{ Vm/N}$			
Density, ρ_{pe}	7800kg/m^3			
Piezoelectric compliance, $s_{11,p}$	$15 \times 10^{-12} \mathrm{m}^2/\mathrm{N}$			
Relative Dielectric constant, K_3^T or $(1/(\beta_p \epsilon_0))$ 1800				
TdVib Ga	alfenol			
Piezomagnetic coefficient, $d_{33,m}$	15–30 nm/A (15 used)			
Density, ρ_{ms} 7800 kg/m				
Magnetostrictive compliance, s_{33}^H 12.5–25.0 × 10 ⁻¹² m ² /N (16				

Table 4. Material properties used for Metglas-PVDF model [25,29].

Property	Value			
TE Metallized PVDF				
Piezoelectric voltage coefficient, $g_{31,p}$ Density, ρ_{pe} Piezoelectric compliance, $s_{11,p}$ Relative Dielectric constant, K_3^T or $(1/(\beta_p \epsilon_0))$	$216 \times 10^{-3} \text{ Vm/N}$ 1780 kg/m^3 $3.7 \times 10^{-10} \text{ m}^2/\text{N}$ 12			
Metglas 2605	SA1			
Piezomagnetic coefficient, $d_{33,m}$ Density, ρ_{ms} Magnetostrictive compliance, s_{33}^H	25–50 nm/A (25 used) 7180 kg/m $9.09 \times 10^{-12} \text{ m}^2/\text{N}$			

Table 5. Optimization results.

Optimized Parameter	ME Galfenol-PZT		ME Metglas-PZT		MME PZT Bimorh	
	ICNIRP	IEEE	ICNIRP	IEEE	ICNIRP	IEEE
$l=2l_0$	21.5 mm	2 mm	25.2 mm	2 mm	NA	NA
t_P	15.9 μm	19.4 μm	18.1 μm	25.5 μm	10 μm	10 μm
t_m	33.5 μm	40.3 μm	22.4 μm	37.3 μm	NA	NA
w	1.1 mm	10 mm	1.26 mm	10 mm	0.4 mm	0.51 mm
H_p	0.44 Oe	2.89 Oe	0.40 Oe	2.89 Oe	5.56 Oe	38.39 Oe
2Ĺ	NA	NA	NA	NA	8.0 mm	8.0 mm
L_m	NA	NA	NA	NA	0.48 mm	0.39 mm
h	NA	NA	NA	NA	5.0 mm	5.0 mm
ω_1	65 kHz	698 kHz	71.9 kHz	915 kHz	61 Hz	325 Hz
P_{avg}	15.6 μW	7.4 mW	62.6 μW	42.7 mW	120 μW	8.7 mW

The MME optimization was performed over the following five variables: beam length (or half transducer length) (L), beam width (w), piezoelectric thickness (t_p), magnet length (L_m), and magnet height (h). Both the operating frequency (ω) and load resistance (R_l) were calculated with closed form solutions as the six optimization parameters completely determine these two parameters. The PZT material was assumed to be PZT-5A with the same properties as in Table 3. The magnet was assumed to be Neodymium N52 with a remanant polarization of 1.46 Tesla and a density of 7500 kg/m³. As with the ME devices, the optimization was performed with the ICNIRP standard, IEEE standard, and a 1 Oe peak limitation at any frequency. The mechanical quality factor (Q_m) was set to 42 based on experimental results. The results of the optimization are shown in Table 5.

4. Discussion

Consider the two material sets used for the ME optimization (see Table 5). For all 3 magnetic field constraint conditions, the Metglas-PZT system outperforms the Galfenol-PZT system. Metglas has a higher magnetostrictive coefficient and is stiffer than Galfenol. This difference allows for greater device extension and a thicker piezoelectric layer thickness relative to the magnetostrictive layer. In addition, Metglas requires a much lower DC bias field, which makes it the clear choice for this application.

The IEEE and ICNIRP standards lead to very different optimal ME beam geometries. The IEEE standard leads to a short, wide, and thick structure ($l_0 = 1 \text{ mm}$, w = 10 mm, $t_t = 0.1 \text{ mm}$ for Metglas-PZT). From 3.35 kHz to 3 MHz, the magnetic field allowed by the IEEE standard is constant. As power generation will scale with the operational frequency and square of the magnetic field amplitude, the optimization will naturally try to maximize the resonance frequency of the ME structure. The optimization routine also selects a design that maximizes the transducer volume as would be expected. Therefore, as mass is more or less constant, the remaining opportunity for increased power is to increase stiffness within allowable constraints resulting in a short/wide beam. The power output results of this geometry (42.7 mW) are very promising.

As seen in Figure 14, the allowable magnetic field under the ICNIRP standard is constant from 0.82 to 65 kHz, above which point the allowable field decreases at a rate of approximately 20 dB per decade. Following the same scaling logic, one would expect the optimization routine to select a maximum volume design that operates at the 65 kHz discontinuity in the allowable field. In fact, the optimizer does select a design very close to this operating point (71.9 kHz). In order to maintain maximum volume within allowable geometric constraints, the resulting structure is a long and narrow structure ($l_0 = 12.6$ mm, w = 1.26 mm, $t_t = 0.063$ mm for Metglas-PZT) in contrast to the structure constrained by the IEEE standard. The estimated power generated (62.6 μ W) is enough for many wireless sensing applications, but certainly not as promising as the estimated power output resulting from the IEEE standard. Finally, the maximum material stresses generated for the ME device designs for each safety constraint were calculated and found to be at least an order of magnitude below the fracture stress (50–70 MPa [30]).

The MME architecture results in a structure with a far lower resonance frequency given that the transducer is excited in a bending vibration mode rather than in an extensional mode. Therefore, the MME device designs will generally be between 10's of Hz and 1 kHz. Referring again to Figure 14, the allowable magnetic field under the IEEE standard for this frequency range is constant while the allowable field under the ICNIRP standard decreases at about 20 dB per decade. Therefore, the same scaling effects are at play with regard to the optimization algorithm. Under the IEEE standard constraint, the optimizer tends to shorten the beam to increase the resonance frequency. Under the ICNIRP standard constraint, the optimizer tends to lengthen the beam to increase the allowable magnetic field by decreasing the resonance frequency. A somewhat arbitrary height limit of 5 mm was placed on the magnet. In all cases, the optimization routine selects the maximum thickness magnet which increases the moment applied to the beam and therefore the stress and generated electric field in the PZT. Given this height constraint, the estimated power under the IEEE standard is about 5 times lower than the ME device (8.7 compared 42.7 mW). However, under the ICNIRP standard, the MME device estimated power actually goes up by about a factor of 2 (120 compared to 62.6 µW). This can be explained by the larger difference in allowable magnetic field as frequency decreases for the ICNIRP standard. However, two complicating factors should be discussed. First, the maximum stress in the PZT material for the MME device is 195 MPa and 37 MPa under the IEEE and ICNIRP standards, respectively. The fracture stress for PZT-5A is approximately 50–70 MPa. So, this MME-IEEE device would certainly fail. The MME-ICNIRP device would also be suspect given fatigue constraints. In order to reduce the stress generated, either the magnet height or the applied magnetic field needs to be reduced. Either of these options results in lower power output. Secondly, as previously discussed, the design that optimizes power output reduces the substrate thickness to zero meaning that bending beam is entirely made of piezoelectric material which is brittle. A thin piezoelectric beam with a large

Materials 2019, 12, 512 17 of 18

attached proof mass and no substrate between piezoelectric layers will almost certainly fracture in the presence of even a fairly mild shock. Therefore, to achieve a robust design a substrate needs to be added which would further reduce power output. Given these two complicating factors it appears that an ME architecture would almost always make a superior wireless power receiver.

5. Conclusions

The goal of this work was to investigate competing wireless power receiver concepts specifically applied to the size and safety constraints demanded for implantable medical devices (IMDs). Because the efficiency of traditional coil to coil wireless power transfer drops dramatically as size decreases, magnetoelectric (ME) and mechano-magnetoelectric (MME) receiver transducers were considered. Lumped element models were developed for each type of receiver that can be useful design aids in applications not only for IMDs, but also for wireless sensors and wearable sensors in general. These models were experimentally verified and subsequently used to produce optimized designs for an overall size constrain of 2 mm³. Two different safety standards, the IEEE [22,23] and ICNIRP [24], were used as constraints to the optimization process. The results of this study reveal that the ME architecture is definitely preferable under the IEEE standard and given practical constraints is also preferable under the ICNIRP standard, although in the latter case, the estimated power produced by each type of structure is similar. The optimized ME devices are estimated to produce 42.7 mW (21.35 mW/mm³) and 62.6 μ W (31.3 μ W/mm³) under the IEEE and ICNIRP standard, respectively. Although much work needs to be done to implement transducers of this size and performance level, these results are very promising in the context of being able to wirelessly power very small biomedical implants.

Author Contributions: T.R. and S.R. designed the project; T.R. developed ME lumped element model, B.D.T. carried out MME lumped element model and T.R. performed simulations; T.R. and S.W. performed experiments and analyzed results; T.R. and S.R. wrote the manuscript.

Funding: This research was funded by the National Science Foundation under Award Number ECCS-1651438.

Conflicts of Interest: The authors declare no conflict of interest.

References

- 1. Song, S.H.; Kim, A.; Ziaie, B. Omni-Directional Ultrasonic Powering for mm-Scale Implantable Biomedical Devices. *IEEE Trans. Biomed. Eng.* **2015**, *62*, 2717–2723. [CrossRef] [PubMed]
- 2. Basaeri, H.; Christensen, D.B.; Roundy, S. A review of acoustic power transfer for bio-medical implants. *Smart Mater. Struct.* **2016**, *25*, 123001. [CrossRef]
- 3. Amar, A.B.; Kouki, A.B.; Cao, H. Power approaches for implantable medical devices. *Sensors* **2015**, *15*, 28889–28914. [CrossRef] [PubMed]
- 4. Abiri, P.; Abiri, A.; Packard, R.R.S.; Ding, Y.; Yousefi, A.; Ma, J.; Bersohn, M.; Nguyen, K.-L.; Markovic, D.; Moloudi, S.; et al. Inductively powered wireless pacing via a miniature pacemaker and remote stimulation control system. *Sci. Rep.* **2017**, *7*, 6180. [CrossRef] [PubMed]
- 5. Denisov, A.; Yeatman, E. Ultrasonic vs. Inductive Power Delivery for Miniature Biomedical Implants. In Proceedings of the 2010 International Conference on Body Sensor Networks, Singapore, 7–9 June 2010; pp. 84–89.
- 6. Fiebig, M. Revival of the magnetoelectric effect. J. Phys. D Appl. Phys. 2005, 38, R123–R152. [CrossRef]
- 7. Dzyaloshinskii, I. On the magneto-electrical effect in antiferromagnets. Sov. Phys. JETP 1959, 37, 881.
- 8. Tellegen, B.D. The Gyrator, a New Electric Network Element. *Philips. Res. Rep.* **1948**, *3*, 81–101.
- 9. Nan, C.W. Magnetoelectric effect in composites of piezoelectric and piezomagnetic phases. *Phys. Rev. B* **1994**, 50, 6082. [CrossRef]
- 10. Shin, K.H.; Inoue, M.; Arai, K.I. Preparation and properties of elastically coupled electro-magnetic elements with a bonding structure. *IEEE Trans. Magn.* **1998**, *34*, 1324–1326. [CrossRef]
- 11. Ryu, J.; Carazo, A.V.; Uchino, K.; Kim, H.E. Magnetoelectric properties in piezoelectric and magnetostrictive laminate composites. *Jpn. J. Appl. Phys.* **2001**, *40*, 4948. [CrossRef]

12. Zhai, J.; Xing, Z.; Dong, S.; Li, J.; Viehland, D. Magnetoelectric laminate composites: An overview. *J. Am. Ceram. Soc.* **2008**, *91*, 351–358. [CrossRef]

- 13. Dong, S.; Cheng, J.; Li, J.F.; Viehland, D. Enhanced magnetoelectric effects in laminate composites of Terfenol-D/Pb(Zr,Ti)O₃ under resonant drive. *Appl. Phys. Lett.* **2003**, *83*, 4812–4814. [CrossRef]
- 14. Dong, S.; Li, J.F.; Viehland, D. Characterization of magnetoelectric laminate composites operated in longitudinal-transverse and transverse-transverse modes. *J. Appl. Phys.* **2004**, *95*, 2625–2630. [CrossRef]
- Dong, S.; Li, J.F.; Viehland, D. Longitudinal and transverse magnetoelectric voltage coefficients of magnetostrictive/piezoelectric laminate composite: Theory. *IEEE Trans. Ultrason. Ferroelectr. Freq. Control* 2003, 51, 794–799. [CrossRef]
- 16. Paprotny, I.; Xu, Q.; Chan, W.W.; White, R.M.; Wright, P.K. Electromechanical energy scavenging from current-carrying conductors. *IEEE Sens. J.* **2013**, *13*, 190–201. [CrossRef]
- 17. Han, J.; Hu, J.; Wang, Z.; Wang, S.X.; He, J. Enhanced performance of magnetoelectric energy harvester based on compound magnetic coupling effect. *J. Appl. Phys.* **2015**, *117*, 144502. [CrossRef]
- 18. Truong, B.D.; Roundy, S. Wireless Power Transfer System with Center Clamped Magneto-Mechano-Electric (MME) Receiver: Model Validation and Efficiency Investigation. *Smart Mater. Struct.* **2018**, *28*, 015004. [CrossRef]
- 19. O'Handley, R.C.; Huang, J.K.; Bono, D.C.; Simon, J. Improved Wireless, Transcutaneous Power Transmission for In Vivo Applications. *IEEE Sens. J.* **2008**, *8*, 57–62. [CrossRef]
- 20. Paluszek, M.; Avirovik, D.; Zhou, Y.; Kundu, S.; Chopra, A.; Montague, R.; Priya, S. Magnetoelectric composites for medical application. In *Composite Magnetoelectrics: Materials, Structures, and Applications*; Srinivasan, G., Priya, S., Sun, N.X., Eds.; Woodhead Publishing: Sawston, UK, 2005; p. 381.
- 21. Yang, G.; Talleb, H.; Gensbittel, A.; Ren, Z. FEM Modeling of a Magnetoelectric Transducer for Autonomous Micro Sensors in Medical Application. *Sens. Imaging* **2015**, *16*, 12. [CrossRef]
- 22. IEEE C95.1-2005. IEEE Standard for Safety Levels with Respect to Human Exposure to Radio Frequency Electromagnetic Fields, 3 kHz to 300 GHz; IEEE: Piscataway, NJ, USA, 2006.
- 23. IEEE International Committee and E. S. on N.-I. Radiation. *IEEE Standard for Safety Levels with Respect to Human Exposure to Electromagnetic Fields*, 0–3 kHz; IEEE: Piscataway, NJ, USA, 2007.
- 24. International Commission on Non-Ionizing Radiation Protection. ICNIRP Guidelines for Limiting Exposure to Time-Varying Electric, Magnetic and Electromagnetic fields. *Health Phys.* **1998**, 74, 494–522.
- 25. Zhai, J.; Dong, S.; Xing, Z.; Li, J.; Viehland, D. Giant magnetoelectric effect in Metglas/polyvinylidene-fluoride laminates. *Appl. Phys. Lett.* **2006**, *89*, 1–4. [CrossRef]
- 26. Zhou, Y.; Yang, S.C.; Apo, D.J.; Maurya, D.; Priya, S. Tunable self-biased magnetoelectric response in homogenous laminates. *Appl. Phys. Lett.* **2012**, *101*, 232905. [CrossRef]
- 27. Nan, C.W.; Bichurin, M.I.; Dong, S.; Viehland, D.; Srinivasan, G. Multiferroic magnetoelectric composites: Historical perspective, status, and future directions. *J. Appl. Phys.* **2008**, *103*. [CrossRef]
- 28. Bian, L.; Wen, Y.; Li, P.; Gao, Q.; Zheng, M. Magnetoelectric transducer with high quality factor for wireless power receiving. *Sens. Actuators A Phys.* **2009**, *150*, 207–211. [CrossRef]
- 29. Freeman, E.; Harper, J.; Goel, N.; Gilbert, I.; Unguris, J.; Schiff, S.J.; Tadigadapa, S. Improving the magnetoelectric performance of Metglas/PZT laminates by annealing in a magnetic field. *Smart Mater. Struct.* 2017, 26, 085038. [CrossRef] [PubMed]
- 30. Kornmann, X.; Huber, C. Microstructure and mechanical properties of PZT fibres. *J. Eur. Ceram. Soc.* **2004**, 24, 1987–1991. [CrossRef]



© 2019 by the authors. Licensee MDPI, Basel, Switzerland. This article is an open access article distributed under the terms and conditions of the Creative Commons Attribution (CC BY) license (http://creativecommons.org/licenses/by/4.0/).